THE JOURNAL OF PHYSICAL CHEMISTRY Letters
Cite This: J. Phys. Chem. Lett. 2018, 9, 3043−3048
Letter
pubs.acs.org/JPCL

Unravelling the Photoprotection Properties of Mycosporine Amino Acid Motifs

Jack M. Woolley, Michael Staniforth, Michael D. Horbury, Gareth W. Richings, Martin Wills, and Vasilios G. Stavros*

Department of Chemistry, University of Warwick, Gibbet Hill Road, Coventry CV4 7AL, U.K.

Supporting Information

ABSTRACT: Photoprotection from harmful ultraviolet (UV) radiation exposure is a key problem in modern society. Mycosporine-like amino acids found in fungi, cyanobacteria, macroalgae, phytoplankton, and animals are already presenting a promising form of natural photoprotection in sunscreen formulations. Using time-resolved transient electronic absorption spectroscopy and guided by complementary *ab initio* calculations, we help to unravel how the core structures of these molecules perform under UV irradiation. Through such detailed insight into the relaxation mechanisms of these ubiquitous molecules, we hope to inspire new thinking in developing next-generation photoprotective molecules.

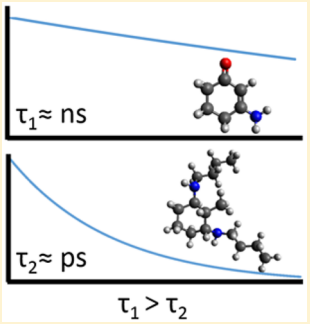

Identification of ultraviolet radiation-absorbing molecules within natural environments[1−4] has led to elevated interest into their relative photostabilities[5−8] as they can play a crucial role in photoprotection. Two such classes of natural photoprotective molecules are mycosporines and mycosporine-like amino acids (herein referred to as MAAs).[1,9] Such molecules are ubiquitous in nature commonly found in fungi, cyanobacteria, macroalgae, phytoplankton and accumulated through ingestion in high-order animals.[1,10,11] Furthermore, they are used as active ingredients in commercial sunscreen products.[12] MAAs exhibit a strong absorption band in the UVA/UVB region of the electromagnetic spectrum (400−315 nm UVA, 315−280 nm UVB). They share a common cyclohexenone or cyclohexenimine core, with their additional functional groups determining the specific absorption maximum. While many articles exist exploring the presence and extraction of MAAs,[4,13−16] experimental information pertaining to their ultrafast photophysics and photochemistry within the first few picoseconds following photoexcitation is, to the best of our knowledge, lacking. This information, along with complementary studies of longer (nanosecond) temporal duration,[11,17,18] can provide greater insight into the molecules' ability to provide photoprotection.

Recent *ab initio* calculations on porphyra-334 and palythine, two commonly found MAAs, suggest that after UV absorption, these MAAs undergo a rapid internal conversion to the electronic ground (S_0) state.[17,19] This leads to effective dissipation of the UV photon energy as heat. These conclusions have been corroborated through photoacoustic calorimetry studies, which demonstrate that a significant amount of photon energy (greater than 90%) is delivered to the surrounding environment,[17,18] reducing the probability of potentially dangerous photoreactions occurring. Analogues of several MAAs have been recently suggested as suitable synthetic replacements in commercial products and studied both through steady-state absorption measurements and theoretically,[20] as extraction or synthesis yields only small quantities of the natural MAAs.[1,21,22] Indeed, the recent theoretical work has explored the excited-state potential energy landscape of a selection of model MAA analogues.[20] These studies indicate that upon photoexcitation of molecules containing a cyclohexenone core, the population travels along the excited-state potential before becoming trapped within the excited-state minimum. For those that have a cyclohexenimine core, photoexcitation to the first excited-state is followed by rapid relaxation along an out-of-plane flexing motion, leading to an accessible conical intersection (CI) promoting ground-state repopulation, consistent with previous theoretical studies on palythine.[19]

To shed further insight into these excited-state decay pathways, we employed femtosecond (fs) time-resolved transient electronic (ultraviolet−visible or UV−vis) absorption spectroscopy (TEAS) combined with a molecular "bottom-up" approach,[23] to study simplified chromophore subunits (*i.e.*, motifs) of MAAs. The systems we have chosen to act as analogues are 3-aminocyclohex-2-en-1-one (termed **ACyO**) and (Z)-N-(3-(butylamino)-2-methylcyclohex-2-en-1-ylidene)-butan-1-aminium 4-methylbenzenesulfonate (termed **NN**), and both are shown as insets in panels a and b of Figure 1, respectively, alongside their steady-state absorption spectra. These molecules present core structures similar to that of MAAs (Figure 1c,d), and similar species have been explored computationally for their photoprotection capabilities.[20]

Received: March 26, 2018
Accepted: May 11, 2018
Published: May 11, 2018

DOI: 10.1021/acs.jpclett.8b00921
J. Phys. Chem. Lett. 2018, 9, 3043−3048

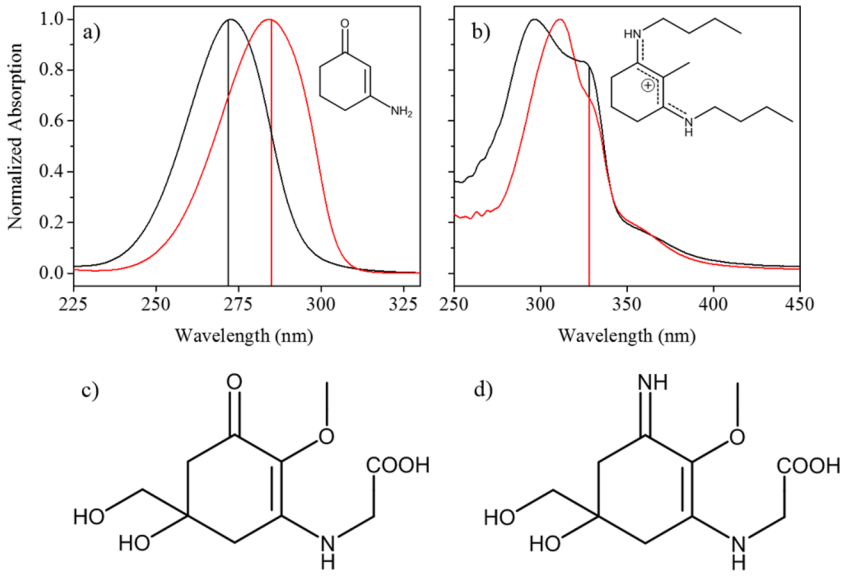

Figure 1. Steady-state absorption spectra of (a) **ACyO** (inset) and (b) **NN** (inset), in methanol (red line) and acetonitrile (black line). Vertical lines indicate photoexcitation wavelength for each solvent. Two common MAAs are also displayed: (c) mycosporine-glycine and (d) palythine.

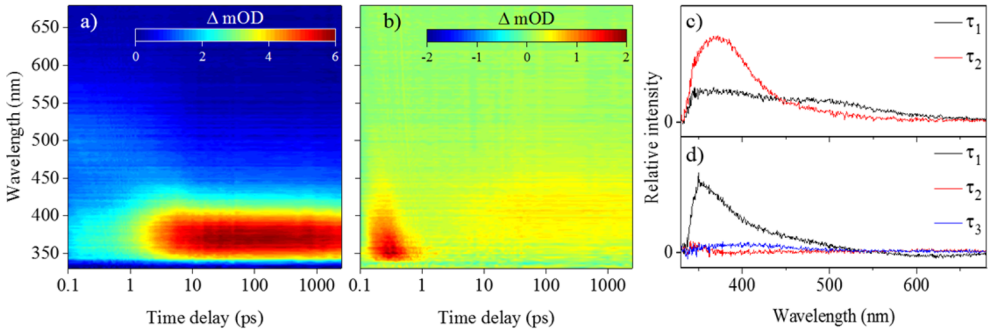

Figure 2. False color maps of TAS of 10 mM **ACyO** in (a) acetonitrile (excitation at 272 nm) and (b) methanol (excitation at 285 nm). Evolution associated difference spectra (EADS) from the global sequential fit (see main discussion) of **ACyO** TAS in (c) acetonitrile and (d) methanol.

We shall first focus on the transient absorption spectra (TAS) of **ACyO** in the polar solvents acetonitrile and methanol (Figure 2). We note here that measurements were also carried out in dioxane, a weakly perturbing, nonpolar solvent, which revealed similar dynamics (see the Supporting Information). We begin with a discussion of **ACyO** (Figure 2a) in acetonitrile, an aprotic polar solvent. Upon photoexcitation at the absorption maximum (λ_{max} = 272 nm; Figure 1a), the initial TAS in acetonitrile (pump−probe time delay (Δt) < 6 ps) displays a broad excited-state absorption spanning from 340 to 600 nm. As Δt increases, the excited-state absorption feature begins to blue shift and narrow, centering at 370 nm with increased intensity. This feature persists to the maximum available Δt of our measurements, which corresponds to 2.5 ns. The TAS of **ACyO** in methanol (Figure 2b; λ_{max} = 285 nm, Figure 1a), a protic polar solvent, displays markedly different features from those of the **ACyO** in acetonitrile (*vide supra*). After initial photoexcitation, the first feature is an intense excited-state absorption peaked around 350 nm which is short-lived (Δt < 1 ps). This short-lived excited-state absorption decays within the first picosecond, leading to the TAS approaching near baseline. Finally, a second, less intense, excited-state absorption feature centered at 400 nm grows in after $\Delta t \sim$ 10 ps, which then persists to the maximum Δt of 2.5 ns.

In comparison to the TAS of **ACyO** in acetonitrile and methanol, the TAS of **NN**, both photoexcited at 328 nm (Figure 1b), do not (visibly) display a dependence on solvent, as evidenced in Figure 3. In addition to a large coherent artifact around Δt = 0 (intense negative feature), the TAS in each solvent show an excited-state absorption, centered at 350 nm (Figure 3a,b), which initially extends to 400 nm then narrows and returns to baseline within 15 ps. Mildly visible in the TAS is a ground-state bleach centered at 340 nm at early time (<1 ps), along with a stimulated emission from 400 nm to the end of the probe region (680 nm). A weak absorption is also visible for the maximum Δt (2.5 ns) centered at 390 nm. These latter features are more apparent in the evolution associated difference spectra (EADS), Figure 3c,d, discussed below.

In order to obtain quantitative insight into the relaxation processes in operation, a global fitting technique using the software package Glotaran[24] was employed on the TAS of **ACyO** and **NN** in acetonitrile and methanol. Each TAS was fitted to a sequential model ($A \xrightarrow{\tau_1} B \xrightarrow{\tau_2} C \ldots$). The extracted time constants, τ_n, describing the timescale for each step in the relaxation process, are shown in Table 1. The corresponding EADS are also shown in Figures 2 and 3. The quality of each fit was evaluated through the associated residuals and are presented in the Supporting Information.

DOI: 10.1021/acs.jpclett.8b00921
J. Phys. Chem. Lett. 2018, 9, 3043−3048

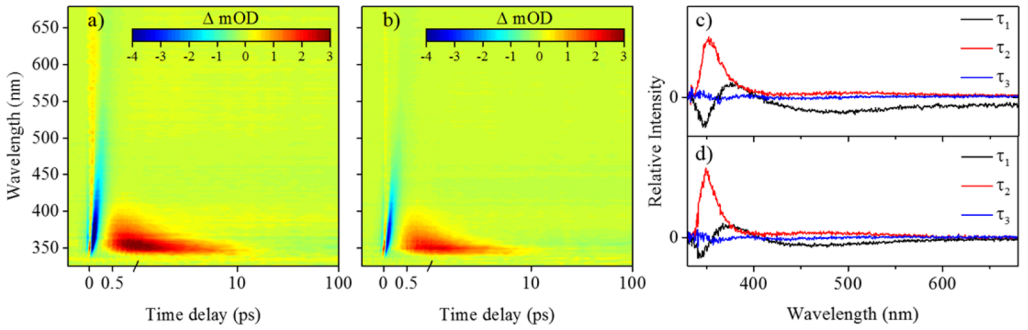

Figure 3. False color maps of TAS of 10 mM **NN** following photoexcitation at 328 nm in (a) acetonitrile and (b) methanol. The pump−probe time delay is plotted linearly from −0.5 to 1 ps and then logarithmically to 100 ps. EADS from the global sequential fit (see main discussion) of **NN** TAS in (c) acetonitrile and (d) methanol.

We now assign processes to the dynamical time constants starting with **ACyO** in acetonitrile. We use previous studies to aid our discussion, where appropriate. *Ab initio* calculations[25] have shown that excitation at the absorption maximum, a $^1\pi\pi^*$ transition, leads to population of the first singlet excited-state (S_1). From the EADS presented in Figure 2c, we see that the broad excited-state absorption described by τ_1 at early time is sensibly consistent with a vibrationally hot S_1 population, which undergoes vibrational energy transfer, both intramolecular and intermolecular (to the solvent), with a time constant of $\tau_1 \approx 3$ ps. The now narrower EADS associated with τ_2 is assigned to a vibrationally cold population trapped within the minimum of the S_1 excited-state, which persists beyond the temporal duration of the experiment (Δt = 2.5 ns). In keeping with recent theory calculations mapping the potential energy surface of the excited-state of cyclohexenone units, we thus propose that as the molecule moves along the S_1 potential energy surface, from the initially populated Franck−Condon region, sufficient energy is lost to the surrounding solvent environment such that the excited-state population is energetically removed from the CI and thus trapped on the S_1 minimum.[20] We draw confidence in this comparison through complementary calculations we have carried out (see the Supporting Information for details). Importantly, our complete active space self-consistent fields calculations at critical points along the S_1 surface (S_1 minimum and S_1/S_0 CI) reveal that mild modifications to the geometric structure (absence of methyl on the nitrogen, Figure 1a) appear to have little effect on the electronic structure (see the Supporting Information for details), adding credence to the comparison between the present experiment and previous theory.[20]

ACyO in methanol displays different features in the TAS at early Δt and requires three time constants to model the TAS. The corresponding EADS are shown in Figure 2d. The first EADS associated with τ_1 (330 fs), which has an excited-state absorption feature peaking at 350 nm, can likely be attributed to a fast geometry relaxation on S_1, along with any solvent rearrangement. With regard to the second EADS, associated with τ_2 (3.4 ps), we attribute this to excited-state population vibrationally cooling, *via* vibrational energy transfer, as it traverses along the excited-state potential, ultimately finding its way to the minimum of the S_1. This population persists with a time constant (τ_3) greater than the maximum Δt of our experiment.

Two points are worthy of note with regard to the EADS collated for **ACyO** in methanol. First, the EADS associated with τ_3 is far less intense than the EADS associated with τ_1 (*cf.* when using an aprotic solvent, the opposite is the case). We surmise this is likely due to the stronger perturbations to the electronic structure, induced by the protic solvent, which will inevitably modify the excited-state absorption accordingly. Second, the need for an intermediate (τ_2) dynamical component again highlights the perturbation induced by the protic solvent. One could speculate that following evolution from the Franck−Condon region, the excited-state population encounters a region on the potential energy surface where the excited-state absorption drops considerably, or there is strong excited-state absorption *and* stimulated emission in competition (we see evidence of the latter in the EADS (τ_1)). This leads to almost baseline recovery in the TAS for **ACyO** in methanol (Figure 2b) observed between 1 and 5 ps (*i.e.*, during vibrational energy transfer). This competition of excited-state absorption and stimulated emission could also artificially reduce τ_1, over the region. Once out of this region, the stimulated emission decreases, or the excited-state absorption increases (or both) across this spectral region.

We finally conclude our discussion on the **ACyO** data by noting that for both aprotic and protic solvents, we would anticipate radiative decay from a long-lived excited-state, however, none was observed. The calculated gas-phase transition dipole moment between the S_1 minimum and ground electronic state (S_0) was determined to be 0.0019 D, which sensibly agrees with the absence of any fluorescence signature.

Global fitting of **NN** in acetonitrile and methanol required three time constants with associated EADS shown in Figure 3c,d; the time constants are also shown in Table 1. The EADS associated with τ_1 (≈500 fs in both solvents) consist of a ground-state bleach centered on 340 nm and an excited-state absorption peaking at 375 nm along with a shallow stimulated emission (approximately 400−680 nm). The dynamical processes responsible for these EADS are assigned to **NN**

Table 1. Time Constants and Associated Errors (2σ) Extracted from the Sequential Fit for ACyO and NN in Acetonitrile and Methanol

	τ_1	τ_2	τ_3
ACyO			
acetonitrile	2.80 ps ± 200 fs	≫2.5 ns	–
methanol	330 fs ± 40 fs	3.40 ps ± 300 fs	≫2.5 ns
NN			
acetonitrile	440 fs ± 40 fs	2.49 ps ± 40 fs	≫2.5 ns
methanol	680 fs ± 40 fs	1.52 ps ± 100 fs	≫2.5 ns

DOI: 10.1021/acs.jpclett.8b00921
J. Phys. Chem. Lett. 2018, 9, 3043−3048

undergoing a fast geometry relaxation on S_1, along with excited-state population traversing through the S_1/S_0 CI. The time constant (τ_1) for this EADS compares judiciously to dynamical calculations reported for similar type systems.[20] One might expect the stimulated emission to red-shift, as the excited-state population traverses the S_1 potential energy surface on route to the CI. Such a red-shift is potentially observable from the TAS. However, the presence of the excited-state absorption at early times (positive feature at 375 nm) and its evolution as excited-state population moves toward the CI, likely obscuring this red-shift. This limits our ability to confidently track population-flow along the S_1 surface. The second EADS associated with time constant τ_2 (= 2.49 ps in acetonitrile and = 1.52 ps in methanol) are attributed to vibrational cooling, *via* vibrational energy transfer, of the vibrationally hot (now) S_0 state. From the TAS in Figure 3a,b, this is clearly manifested as a characteristic blue-shift of the absorption feature, as the excited-state absorption returns to baseline.[26,27] The final EADS associated with time constant τ_3 describe the evolution of a weak excited-state absorption. This excited-state absorption may be reconciled by invoking a long-lived triplet state, or the appearance of a photoproduct.[8,18]

To summarize, the excited-state dynamics of **ACyO** in both aprotic (acetonitrile) and protic (methanol) solvents show that a long-lived S_1 state persists beyond the maximum Δt of the experiment and is assigned a time constant $\gg$2.5 ns. At early time delays, the spectral responses differ between **ACyO** in acetonitrile and methanol, the former showing vibrational cooling to a minimum of the S_1 potential in 2.8 ps, while in the latter, the initial time constant of 330 fs is attributed to geometry relaxation and solvent rearrangement, followed by vibrational cooling within 3.4 ps, again leading to a long-lived population in the S_1 minimum. This is consistent with our own, as well as previously reported theoretical work.[20] Combined, this suggests that excited-state properties of cyclohexenone-based systems prevent effective repopulation of the electronic ground state on an ultrafast time-scale due to the S_1/S_0 CI being energetically inaccessible (see the Supporting Information). This is schematically shown in Figure 4a. These results

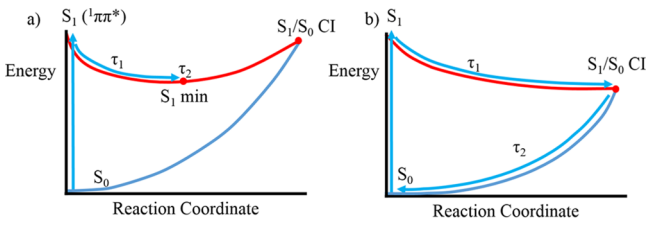

Figure 4. Schematic of potential energy surfaces for **ACyO** in (a) acetonitrile and (b) **NN**. Note τ_3 for **NN** has been omitted for clarity. Adapted with permission from ref 20. Copyright 2017 Wiley.

imply that cyclohexenone-based systems should perform poorly as a photoprotective molecule because of the long-lived excited-state, increasing the likelihood for potentially harmful photochemical reactions.[28] However, prior studies on gadusol, mycosporine-glycine, and mycosporine-glutaminol-glucoside, all of which have a cyclohexanone core, demonstrate a high level of photostability.[29−31] This is likely due to the absence of a localized energy minimum in the S_1 state before the S_1/S_0 CI, as seen in gadusol,[32] and evidenced in the present studies on **NN**. Therefore, the photostability of cyclohexenone-based systems is due to additional functional groups present, rather than an intrinsic property of the cyclohexanone core. We add here the potential importance of the methoxy group at the *ortho* position (Figure 1c,d), as many MAAs possess this functionality at this position.[9] Such a finding therefore lends itself to further studies exploring the degree of functionalization (as well as the nature of the functionalities) required to induce photostability to the cyclohexenone core.

In comparison, **NN** displays electronic excited-state dynamics which are largely independent of solvent environment. From the initial photoexcited population, the system returns to a vibrationally hot S_0 state in ≈500 fs. Once in the vibrationally hot S_0 state, the timescales for vibrational relaxation, *via* intermolecular energy transfer to the solvent, do display a dependence upon the solvent environment. The timescale for this vibrational relaxation is shorter in methanol (1.52 ps), a hydrogen-bonding donor and acceptor, compared to acetonitrile (2.49 ps), which is only a hydrogen-bonding acceptor. Interestingly, this correlates well with recent work by Koizumi *et al.*, which demonstrates that hydrogen bonding to the solvent (water) plays a vital role in vibrational relaxation of porphyra-334.[33] This is once again shown schematically in Figure 4b. The remaining photoexcited population persists for the duration of the experiment, either as a populated triplet state or through the formation of a (likely low quantum yield) photoproduct. We add here that the short time scales for vibrational energy transfer in **NN** may be a consequence of its charged nature, which will inevitably influence **NN**−solvent interaction. Importantly, the presently reported dynamics of **NN** show promising properties as a future species of an ultraviolet-absorbing compound. Furthermore, this work also highlights the need to extend these measurements to MAAs themselves, experiments which are currently underway in our laboratory.

EXPERIMENTAL METHODS

Samples of **ACyO** were obtained from Alfa Aesar (95% purity) and prepared in 10 mM concentrations in all solvents (methanol, Fisher Scientific 99%; acetonitrile, Sigma-Aldrich 99%) without any further purification. **NN** was synthesized following a previously reported procedure,[20] briefly described here. To 10 mL of *n*-butylamine (all Sigma-Aldrich) were added 1 mM 2-methyl-1,3-cyclohexanedione and 1 mM *p*-toluenesulfonic acid monohydrate, and the mixture was then refluxed under N_2 for 48 hrs. The resulting solution was concentrated under vacuum and purified through crystallization from CH_2Cl_2 and washed with sequential washes of *n*-hexane. Samples were confirmed through previously reported NMR spectra.[20]

TEAS measurements were recorded at the Warwick Centre for Ultrafast Spectroscopy (WCUS: go.warwick.ac.uk/WCUS) using the following experimental apparatus. The sample was delivered to the interaction region through a demountable liquid cell (Harrick Scientific Products Inc.) at a sample thickness of 100 μm, placed between two CaF_2 windows, and pumped through the cell using a diaphragm pump (SIMDOS 02) at a sufficient rate to ensure that a fresh sample was interrogated at each laser shot. Femtosecond 800 nm pulses (12 W, 1 kHz) were generated by a commercially available, Ti-sapphire regenerative amplified laser system (Spectra-Physics, Dual Ascend Pumped Spitfire Ace) seeded by a Mai Tai (Spectra-Physics). The beam is split into four fractions of approximately equal power, each one having a separate recompression grating. One of these beams (3.5 W) was split once more and utilized to generate the pump and probe beams

DOI: 10.1021/acs.jpclett.8b00921
J. Phys. Chem. Lett. 2018, 9, 3043−3048

for the experiments presented here. A 2.5 W fraction seeds an optical parametric amplifier (Topas-Prime with UV extension, Light Conversion) allowing variability in pump wavelengths to produce a pump beam of 272−328 nm at approximately 600 μW, which is then focused past the sample cell to give a beam diameter of 500 μm at the sample region. To ensure linearity on photon dependence during the TEAS measurements, pump power dependence studies were undertaken (see the Supporting Information). The probe pulses are generated by focusing 5% of the remaining 1 W, 800 nm fundamental beam, which is further attenuated and irised, into a vertically translated CaF_2 window, generating a white light continuum (330−680 nm). The relative polarization between pump and probe pulses was held at magic angle (54.7°) to negate dynamic contributions from molecular reorientation. Pump−probe delays ranging from −1 ps to 2.5 ns are achieved by translating a hollow gold retroreflector on a motorized optical delay line in the probe path (Newport M-IMS500CCHA). Changes in optical density were calculated from the measured probe intensities, collected using a fiber-coupled spectrometer (Avantes, AvaSpec-ULS1650F). Collected TAS were chirp corrected using the KOALA package.[34]

Steady-state UV−vis measurements were carried out on a Lambda 850 spectrophotometer using a quartz cuvette with a 1 cm path length.

■ ASSOCIATED CONTENT

Supporting Information

The Supporting Information is available free of charge on the ACS Publications website at DOI: 10.1021/acs.jpclett.8b00921.

TEAS measurements in nonpolar solvents, fitting residuals for displayed TAS, power dependency measurements for both **ACyO** and **NN**, complete active space self-consistent fields calculations of **ACyO**, NMR of **NN**, and TAS of butan-1-aminium 4-methylbenzenesulfonate (PDF)

■ AUTHOR INFORMATION

Corresponding Author

*E-mail: v.stavros@warwick.ac.uk.

ORCID

Martin Wills: 0000-0002-1646-2379

Vasilios G. Stavros: 0000-0002-6828-958X

Notes

The authors declare no competing financial interest.

■ ACKNOWLEDGMENTS

The authors thank Professor Diego Sampedro for helpful discussions. J.M.W is grateful to EPSRC and Newport Spectra-Physics for a studentship. M.S. thanks the EPSRC for postdoctoral funding (EP/N010825/1). M.D.H. and G.W.R. thank the Leverhulme Trust for postdoctoral funding. V.G.S. is grateful to the EPSRC for an equipment grant (EP/N010825) and the Royal Society and the Leverhulme Trust for a Royal Society Leverhulme Trust Senior Research Fellowship. Computing facilities were provided by the Scientific Computing Research Technology Platform of the University of Warwick.

■ REFERENCES

(1) Bandaranayake, W. M. Mycosporines: Are they Nature's Sunscreens? *Nat. Prod. Rep.* **1998**, *15*, 159−172.

(2) Colabella, F.; Moline, M.; Libkind, D. UV Sunscreens of Microbial Origin: Mycosporines and Mycosporine- like Aminoacids. *Recent Pat. Biotechnol.* **2015**, *8*, 179−193.

(3) Jenkins, G. I. Signal Transduction in Responses to UV-B Radiation. *Annu. Rev. Plant Biol.* **2009**, *60*, 407−431.

(4) Sinha, R. P.; Klisch, M.; Gröniger, A.; Häder, D.-P. Ultraviolet-Absorbing/Screening Substances in Cyanobacteria, Phytoplankton and Macroalgae. *J. Photochem. Photobiol., B* **1998**, *47*, 83−94.

(5) Baker, L. A.; Marchetti, B.; Karsili, T. N. V.; Stavros, V. G.; Ashfold, M. N. R. Photoprotection: Extending Lessons Learned from Studying Natural Sunscreens to the Design of Artificial Sunscreen Constituents. *Chem. Soc. Rev.* **2017**, *46*, 3770−3791.

(6) Baker, L. A.; Horbury, M. D.; Stavros, V. G. Ultrafast Photoprotective Properties of the Sunscreening Agent Octocrylene. *Opt. Express* **2016**, *24*, 10700−10709.

(7) Aloi, A.; Brunetti, A.; Perna, G.; Lasalvia, M.; Capozzi, V.; Tommasi, R. Ultrafast Transient Absorption of Eumelanin Suspensions: The Role of Inverse Raman Scattering. *Biomed. Opt. Express* **2015**, *6*, 4000−4013.

(8) Horbury, M. D.; Baker, L. A.; Rodrigues, N. D. N.; Quan, W.-D.; Stavros, V. G. Photoisomerization of Ethyl Ferulate: A Solution Phase Transient Absorption Study. *Chem. Phys. Lett.* **2017**, *673*, 62−67.

(9) Gao, Q.; Garcia-Pichel, F. Microbial Ultraviolet Sunscreens. *Nat. Rev. Microbiol.* **2011**, *9*, 791−802.

(10) Sinha, R. P.; Singh, S. P.; Häder, D. P. Database on mycosporines and mycosporine-like amino acids (MAAs) in fungi, cyanobacteria, macroalgae, phytoplankton and animals. *J. Photochem. Photobiol., B* **2007**, *89*, 29−35.

(11) Losantos, R.; Sampedro, D.; Churio, M. S. Photochemistry and Photophysics of Mycosporine-Like Amino Acids and Gadusols, Nature's Ultraviolet Screens. *Pure Appl. Chem.* **2015**, *87*, 979−996.

(12) Schmid, D.; Schürch, C.; Zülli, F. Mycosporine-like amino acids from red algae protect against premature skin-aging. *Euro. Cosmet.* **2006**, *9*, 1−4.

(13) Shick, J. M.; Dunlap, W. C. Mycosporine-Like Amino Acids and Related Gadusols: Biosynthesis, Accumulation, and UV-Protective Functions in Aquatic Organisms. *Annu. Rev. Physiol.* **2002**, *64*, 223−262.

(14) Schmidt, E. W. An Enzymatic Route to Sunscreens. *ChemBioChem* **2011**, *12*, 363−365.

(15) Osborn, A. R.; Almabruk, K. H.; Holzwarth, G.; Asamizu, S.; LaDu, J.; Kean, K. M.; Karplus, P. A.; Tanguay, R. L.; Bakalinsky, A. T.; Mahmud, T. De novo synthesis of a sunscreen compound in vertebrates. *eLife* **2015**, *4*, e05919.

(16) Garcia-Pichel, F.; Castenholz, R. W. Occurrence of UV-absorbing, mycosporin-like compounds among cyanobacterial isolates and estimates of their screening capacity. *Appl. Environ. Microbiol.* **1993**, *59*, 163−169.

(17) Conde, F. R.; Churio, M. S.; Previtali, C. M. The deactivation pathways of the excited-states of the mycosporine-like amino acids shinorine and porphyra-334 in aqueous solution. *Photochem. Photobiol. Sci.* **2004**, *3*, 960−967.

(18) Conde, F. R.; Churio, M. S.; Previtali, C. M. Experimental Study of the Excited-State Properties and Photostability of the Mycosporine-Like Amino Acid Palythine in Aqueous Solution. *Photochem. Photobiol. Sci.* **2007**, *6*, 669−674.

(19) Sampedro, D. Computational Exploration of Natural Sunscreens. *Phys. Chem. Chem. Phys.* **2011**, *13*, 5584−5586.

(20) Losantos, R.; Funes-Ardoiz, I.; Aguilera, J.; Herrera-Ceballos, E.; García-Iriepa, C.; Campos, P. J.; Sampedro, D. Rational Design and Synthesis of Efficient Sunscreens to Boost the Solar Protection Factor. *Angew. Chem., Int. Ed.* **2017**, *56*, 2632−2635.

(21) White, J. D.; Cammack, J. H.; Sakuma, K. The Synthesis and Absolute Configuration of Mycosporins. A Novel Application of the Staudinger Reaction. *J. Am. Chem. Soc.* **1989**, *111*, 8970−8972.

(22) White, J. D.; Cammack, J. H.; Sakuma, K.; Rewcastle, G. W.; Widener, R. K. Transformations of Quinic Acid. Asymmetric Synthesis and Absolute Configuration of Mycosporin I and Mycosporin-gly. *J. Org. Chem.* **1995**, *60*, 3600−3611.

DOI: 10.1021/acs.jpclett.8b00921
J. Phys. Chem. Lett. 2018, 9, 3043−3048

(23) Roberts, G. M.; Stavros, V. G. The role of $\pi\sigma^*$ States in the Photochemistry of Heteroaromatic Biomolecules and their Subunits: Insights from Gas-Phase Femtosecond Spectroscopy. *Chem. Sci.* **2014**, *5*, 1698−1722.
(24) Snellenburg, J. J.; Laptenok, S. P.; Seger, R.; Mullen, K. M.; van Stokkum, I. H. M. Glotaran: A Java-Based Graphical User Interface for the R Package TIMP. *J. Stat. Softw.* **2012**, *49*, 1−22.
(25) Sui, X. X.; Li, L.; Zhao, Y.; Wang, H. G.; Pei, K. M.; Zheng, X. Resonance Raman and Density Functional Study of the Excited State Structural Dynamics of 3-amino-2-cyclohexen-1-one in Water and Acetonitrile Solvents. *Spectrochim. Acta, Part A* **2012**, *85*, 165−172.
(26) Anderson, N. A.; Pullen, S. H.; Walker, L. A., II; Shiang, J. J.; Sension, R. J. Ultrafast Polyene Dynamics in Solution: The Conformational Relaxation and and Thermalization of Highly Excited cis-1,3,5-Hexatriene as a Function of Initial Conformation and Solvent. *J. Phys. Chem. A* **1998**, *102*, 10588−10598.
(27) Pecourt, J. M. L.; Peon, J.; Kohler, B. DNA Excited-State Dynamics: Ultrafast Internal Conversion and Vibrational Cooling in a Series of Nucleosides. *J. Am. Chem. Soc.* **2001**, *123*, 10370−10378.
(28) Rodrigues, N. D. N.; Staniforth, M.; Stavros, V. G. Photophysics of Sunscreen Molecules in the Gas Phase: A Stepwise Approach Towards Understanding and Developing Next-Generation Sunscreens. *Proc. R. Soc. London, Ser. A* **2016**, *472*, 20160677.
(29) Moliné, M.; Arbeloa, E. M.; Flores, M. R.; Libkind, D.; Farías, M. E.; Bertolotti, S. G.; Churio, M. S.; van Broock, M. R. UVB Photoprotective Role of Mycosporines in Yeast: Photostability and Antioxidant Activity of Mycosporine-Glutaminol-Glucoside. *Radiat. Res.* **2011**, *175*, 44−50.
(30) Arbeloa, E. M.; Bertolotti, S. G.; Churio, M. S. Photophysics and reductive quenching reactivity of gadusol in solution. *Photochem. Photobiol. Sci.* **2011**, *10*, 133−142.
(31) Rastogi, R. P.; Incharoensakdi, A. Analysis of UV-absorbing Photoprotectant Mycosporine-like Amino Acid (MAA) in the Cyanobacterium Arthrospira sp. CU2556. *Photochem. Photobiol. Sci.* **2014**, *13*, 1016−1024.
(32) Losantos, R.; Churio, M. S.; Sampedro, D. Computational exploration of the photoprotective potential of gadusol. *ChemistryOpen* **2015**, *4*, 155−160.
(33) Koizumi, K.; Hatakeyama, M.; Boero, M.; Nobusada, K.; Hori, H.; Misonou, T.; Nakamura, S. How seaweeds release the excess energy from sunlight to surrounding sea water. *Phys. Chem. Chem. Phys.* **2017**, *19*, 15745−15753.
(34) Grubb, M. P.; Orr-Ewing, A. J.; Ashfold, M. N. R. KOALA: A Program for the Processing and Decomposition of Transient Spectra. *Rev. Sci. Instrum.* **2014**, *85*, 064104.

DOI: 10.1021/acs.jpclett.8b00921
J. Phys. Chem. Lett. 2018, 9, 3043−3048